SiF 2024 – The 13th International Conference on Structures in Fire
University of Coimbra, Portugal, 19 to 21 June 2024

PARAMETRIC NUMERICAL STUDY OF FIRE EXPERIMENTS ON STEEL-CONCRETE COMPOSITE FLOORS

Chenzhi Ma[1],Thomas Gernay[2]

ABSTRACT

Strategies for fire design of steel-concrete composite floors can rely either on fire protection of the individual elements or on alternate load path for structural integrity of the system. This study conducts numerical fire analyses of steel-concrete composite floors to advance understanding of the anticipated performance of the different fire designs. The numerical models were validated against three full-scale fire tests conducted at the NIST. In Test #1, built to prescriptive code for a 2-hour rating of the elements, large crack openings led to flame leak shortly after one hour. The finite element model captured the localized concrete damage and steel mesh fracture observed in the test, confirming the link between the integrity failure and the minimum amount of reinforcement (60 mm^2/m) permitted in current U.S. practice. Test #2 and Test #3 both used 230 mm^2/m of reinforcement, with the latter omitting the fire protection on the central steel beams. The numerical model captured the experimental behavior including stability under 2 hours of ASTM E119 fire and partial deflection recovery during the subsequent cooling phase. A parametric analysis on the slab rebar area shows that the floors with unprotected central beam need a minimum rebar area about 10% (based on S755) greater than those with protected beams. Further, a probabilistic analysis under natural fires indicates that the floors designed to harness system-level membrane behavior have a lower probability of failure than those designed via element-level prescriptive methods with minimum reinforcement.
Keywords: steel-concrete composite floor, full-scale fire test, performance-based fire design, concrete damage, tensile membrane action, fragility curve

1 INTRODUCTION

According to the National Fire Incident Reporting System (NFIRS), between 2012 and 2022, approximately 1.2 million building fires with flames spread beyond the origin of ignition were recorded in the United States (U.S.). These incidents resulted in around 70,000 fire-related injuries. These statistics highlight the significant human and economic cost of fire. Structural fire design is an important layer of safety to mitigate the fire risk. In the U.S., composite steel-concrete floor systems are widely used. Fire protection materials are generally required for the steel members according to the building codes and specifications. However, research over the last thirty years has shown that omitting fireproofing on selected steel members in composite slabs can result in activation of tensile membrane action (TMA) under fire [1]. Performance-based structural fire designs (PBSFD) have therefore relied on TMA for the fire design of composite steel-concrete slabs with unprotected central beams in projects in multiple countries [2]. However, relatively limited research has been conducted in the U.S. with the composite floor detailing specific to this country, and there is a lack of studies characterizing the probabilistic response of these designs.

The National Institute of Standards and Technology (NIST) recently conducted three full-scale experiments on steel-concrete composite floor systems under standard fire [3-5]. The goal was to test the full-scale performance of assemblies typically constructed in the United States and to compare a prescriptive and a

[1] Ph.D. student, Department of Civil and Systems Engineering, Johns Hopkins University,
e-mail: cma31@jhu.edu, ORCID: https://orcid.org/0000-0002-1144-8033
[2] Assistant Professor, Department of Civil and Systems Engineering, Johns Hopkins University
e-mail: tgernay@jhu.edu, ORCID: https://orcid.org/0000-0002-3511-9226

performance-based design. The first experiment was designed per U.S. prescriptive provisions for a 2-hour fire rating, which includes thermal protection on the steel beams and 60 mm^2/m of S755 reinforcement in the concrete slab. The floor slab developed a large crack along the protected secondary beam after about one hour and reached integrity failure well before the 2 hours of standard fire exposure. The second and third experiments were designed with 230 mm^2/m of S480 reinforcement, with the third one omitting the fire protection on the central steel beams to develop tensile membrane action. These second and third experiments showed no failure within 2 hours. Cracks appeared starting at 132 mins in the third test.

The NIST fire tests provided valuable data on the performance of different design methods for composite floor systems in the U.S., and there is an opportunity for further investigation using these data to deepen the understanding and expand on the initial experimental findings. The experimental data can serve to validate the numerical models. These numerical models are then used to conduct detailed analyses, capture a wide range of data in the structure, such as the evolution of damage in concrete and internal forces over time, and conduct parametric analyses. Parametric analyses can serve to determine critical design parameters of the test prototypes, such as the minimum required slab rebar areas, and explore the effects of other design variables or fire exposures. Probabilistic numerical analysis can also be conducted to build fragility curves for the three test prototypes, for functional recovery and lifetime cost analysis.

This paper presents a comprehensive numerical investigation of the NIST full-scale fire experiments, supplemented by parametric and probabilistic analyses. The unique test data are used to validate nonlinear finite element (FE) models and gain further insights into the observed experimental behavior including early cracking and rebar failure of the prescriptive design. Then, the validated models are used to conduct parametric and probabilistic analyses including under natural fires. These numerical data can support improvement of design provisions in U.S. building codes for the fire design of steel-concrete floor systems.

2 NIST FULL-SCALE FIRE TEST

The tested structure was a two-story steel gravity frame with composite floors. It had two bays by three bays in plan, for a total floor area of 18 m × 11 m, see Figure 1. The fire compartment (9.14 m × 6.10 m) was subjected to a total gravity load of 5.2 kPa. The ASTM E119 fire was applied. Detailed information on structural design, construction, and mechanical properties is available in the NIST technical Notes [3-5].

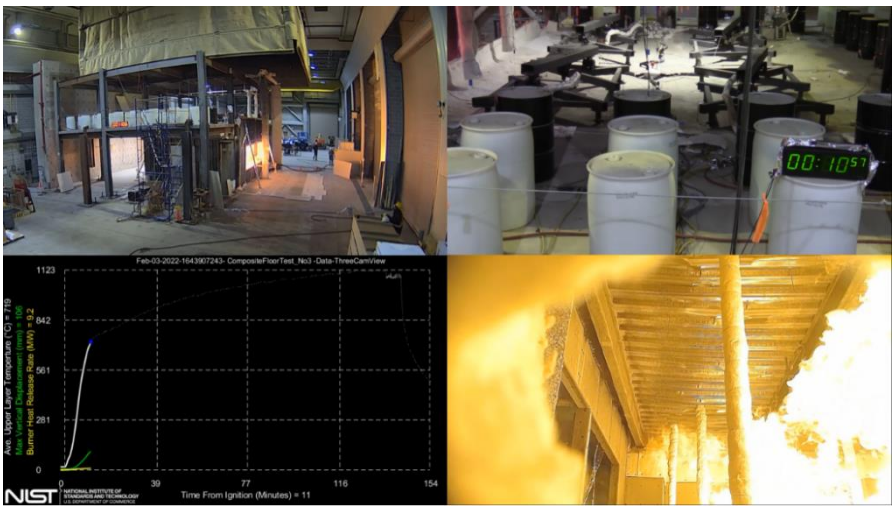

Figure 1. Tested structure and observations during the test [4].

The first experiment with 60 mm^2/m of welded wire mesh reinforcement (755 MPa strength) failed to maintain integrity for 2 hours of standard fire exposure though each individual elements was designed per U.S. prescriptive provisions for a 2-hour fire rating. A full-depth crack appeared above the central beam after approximately one hour of exposure leading to integrity failure.

The second and third experiments were designed with 230 mm^2/m of steel bars reinforcement (480 MPa strength) in the concrete slab in lieu of the minimum 60 mm^2/m wire mesh, and the third experiment had no fire protection on the central steel beam. These second and third experiments showed no failure within 2 hours of exposure, and the third one had its first significant crack after 132 minutes.

3 NUMERICAL MODEL STRATEGY AND VALIDATION

A thermal-structural finite element (FE) model is developed using SAFIR [6] to simulate the behavior of the composite floor systems. Two-dimensional thermal analyses are performed on the sections of the beams and floors using the fire curves obtained from the average temperature of the upper layer in the tests as boundary conditions. Then, a 3D full building model is developed to conduct mechanical analysis.

3.1 Thermal analysis

The computed thermal analysis results for the steel beams and concrete slabs are compared with the test measurements. Temperature-dependent thermal properties of SFRM are adopted from Khorasani et al. [7] (details can be found in [8]). Temperature measurement locations for the beams are shown in Figure 2 (a). In the experiment, temperature readings along the beam length exhibited slight variations, in contrast to the one zone temperatures assumed in the simulation. Figure 3 (a) to (c) compare the steel beam temperature distributions between the test and the simulation for test #1. The temperature distributions in the steel beam computed by SAFIR agree well with the test. The variance in the thin lines, all the same color, represent the temperature measurements taken at different lengths of the beam but at identical sensor positions (e.g., the web), underscoring the spatial differences in the recorded temperatures during the test.

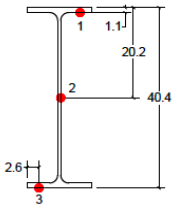

(a) Sensor location in steel beam

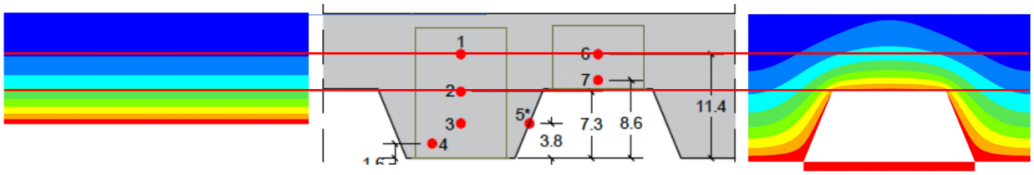

(b) Sensor location in concrete slab and two thermal analysis models (with temperature contour at 95 mins)

Figure 2. Location of thermocouples in the tests and the illustration of two concrete slab models.

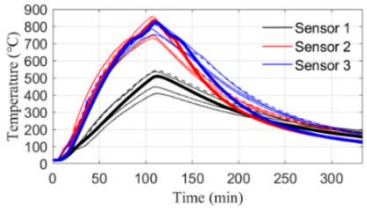

(a) Long primary beam (W16×31)

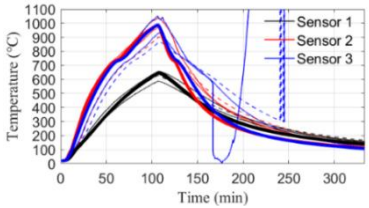

(b) Secondary beam (W16×31)

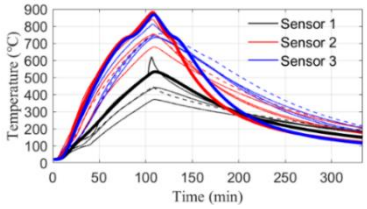

(c) Short primary beam (W18×35)

Figure 3. Comparison between measured and computed temperatures for Test #1 (model: bold lines)

Two modeling strategies are considered for the concrete slab: the first strategy uses the effective thickness approximation where the profiled shape of the slab is simplified based on the approach outlined in the Eurocode EN1994-1-2 Annex D [9]; the second strategy uses the actual geometry of the profiled slab, as shown in Figure 2 (b). The presence of the steel deck is disregarded in the thermal analysis.

3.1.1 Simplified shape concrete thermal analysis

The purpose of simplifying the profiled slab to a rectangular cross section is to facilitate its integration with the structural model, which uses constant thickness thin shell elements. The profiled concrete slab features depths of 158.75 mm and 82.55 mm for its deep and shallow sections, respectively. The effective thickness of the composite slab is 120.65 mm, including 82.55 mm of structural concrete and an additional 38.10 mm of thermal concrete. Figure 4 (a) to (c) compare the temperatures between the measurements and the computed values. The results indicate that the model successfully captured the overall temperature distribution of the slab. Some discrepancies in temperature are observed for the temperature of the reinforcement. In the test, the temperature at the reinforcement steel depth varies between the deep and shallow sections (based on the profiled shape of the deck). In the model, since a constant depth with an effective thickness is considered, the calculated rebar temperature is lower than the measurements taken at shallow sections but higher than those recorded at deep sections. For the same reason, the temperature at the location of sensor 2 is slightly overestimated by the model.

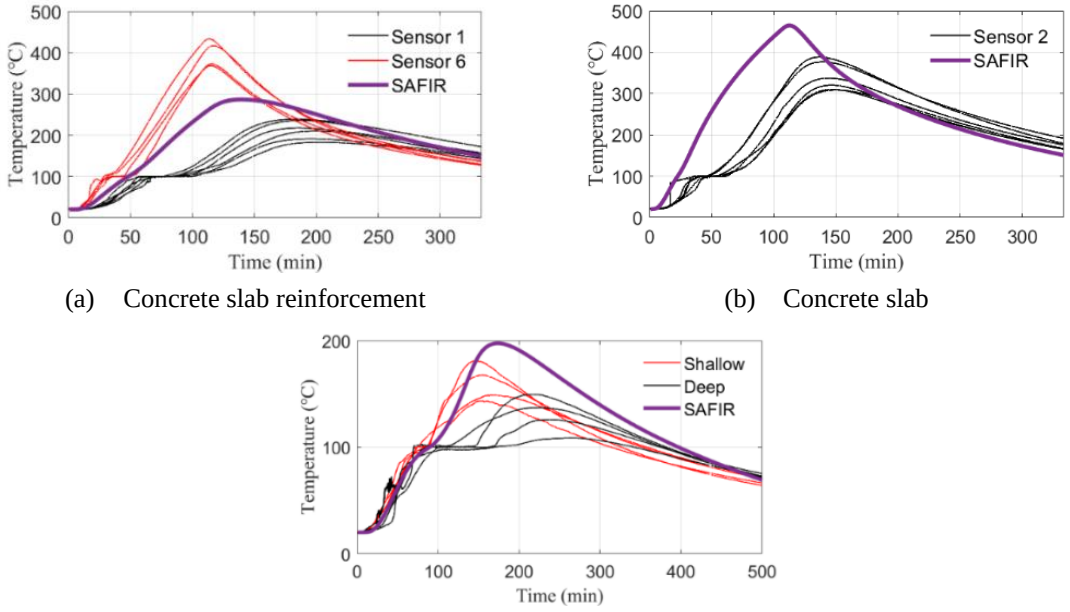

(a) Concrete slab reinforcement

(b) Concrete slab

(c) Slab top temperature

Figure 4. Comparison between measured and computed temperatures for Test #1 with simplified concrete shape (model: bold lines)

3.1.2 Profiled shape concrete thermal analysis

Agreement between computed and measured temperatures can be improved using a more detailed profiled concrete slab model in the thermal analysis [10] as shown in Figure 2 (b). The computed temperatures in the reinforcement are compared with the measured values in Figure 5 (a) The computed values agree with the measured values and the model captures the temperature difference between the shallow and deep sections. Figure 5 (b) and (c) compares the cross-sectional temperatures in both the deep and the shallow sections. The comparison reveals that the computed temperatures are slightly higher than the measured temperatures but still capture the overall temperature distributions.

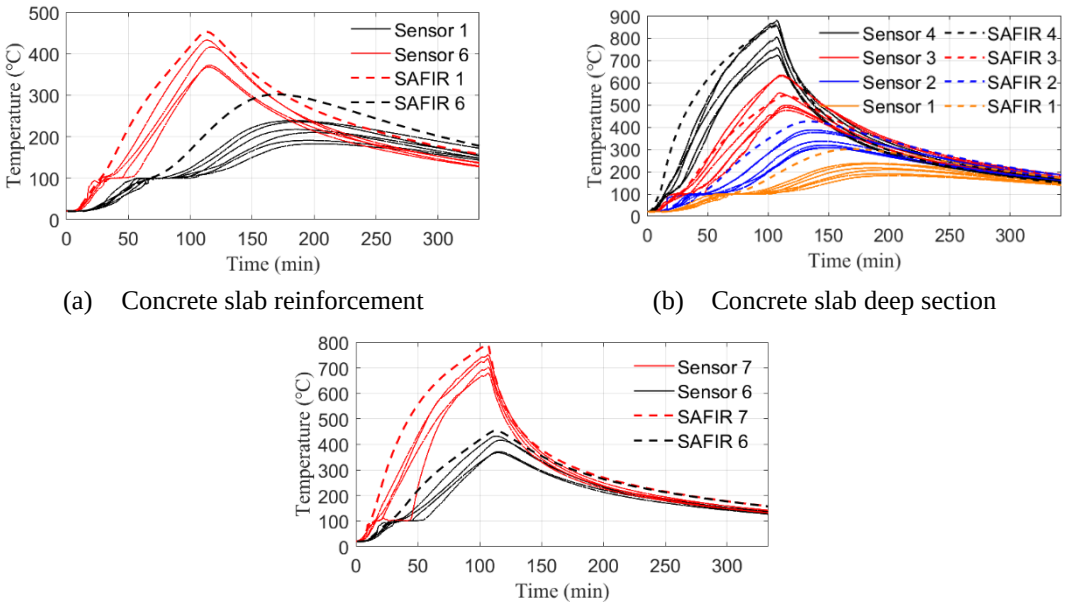

(a) Concrete slab reinforcement

(b) Concrete slab deep section

(c) Concrete slab shallow section

Figure 5. Comparison between measured and computed temperatures for Test #1 with profiled concrete shape (model: dashed lines)

3.2 Mechanical analysis

In the mechanical analysis, a three-dimensional full building model is established, as shown in Figure 6. The boundary conditions of the column ends and beam-column joints align with the test setup. Both the material and geometrical non-linearities and large displacements are considered. The steel deck is conservatively neglected as it is directly exposed to the fire and therefore quickly reaches high temperatures. The material properties used in the model are obtained from the test and their reduction factors at elevated temperatures is in accordance with the Eurocodes. The steel reinforcement is a hot rolled Class A reinforcement according to EN1992-1-2 [11]. The concrete model used with the shell elements is the elevated temperature plastic-damage model with explicit transient creep by Gernay et al. [12]. The reduction of strength with temperature is in accordance with Eurocode. A tensile strength of 1.5 MPa and tensile ductility of 6000 N/m^2, taking into account tension stiffening [13], are adopted. The numerical model is compared to experimental results and observations, focusing on vertical displacements, observed damage patterns within the concrete slab, and the observation at limit states.

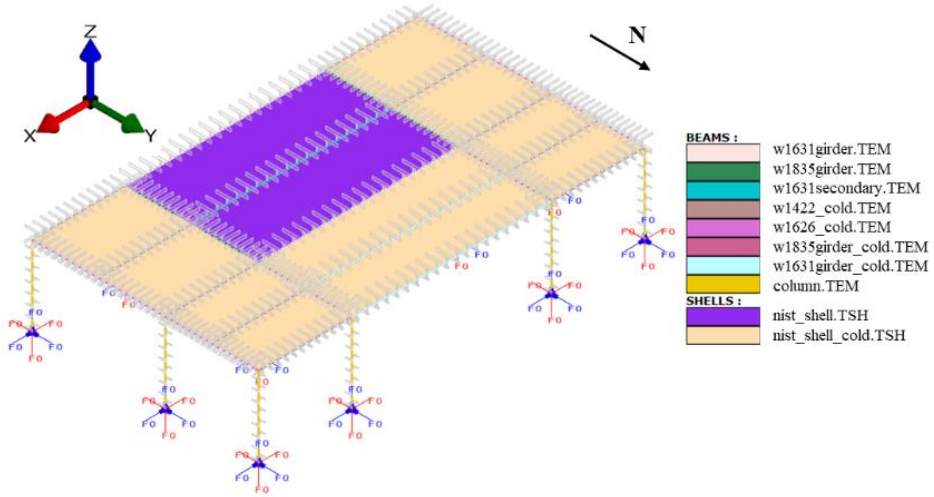

Figure 6. 3D FE model of the tested building in SAFIR (the fire-exposed part of the floor is in purple)

3.2.1 Vertical displacement

Figure 7 plots the vertical displacements at the center of the composite floor system of the three NIST tests, with measurements shown in solid lines and the computed results in dashed lines. The numerical model accurately reflects overall displacement trends and peak values. The model does not fully capture the sudden shifts in displacement rates due to damage, which develop more abruptly in the test. In Test #1, the displacement rose steadily until 69 mins of exposure, then a higher displacement rate was observed due to the development of the full-depth crack above the secondary beam. In the simulation of Test #1, the displacement increases at a constant rate until the peak value, and the simulation stops at 146 mins due to the steel reinforcement failure. Test #2 showed a constant displacement increase rate, captured in the simulation, likely stabilized by the larger rebar area facilitating load transfer across cracks. For Test #3, both test and simulation noted a displacement rate shift at 13 minutes. The initially faster displacements rate was due to the loss of strength of the metal deck and unprotected beam at high temperatures, followed by a slower displacement rate with the activation of tensile membrane action.

Test #2 showed the smallest maximum displacements among the three tests, owing to the enhanced rebar area and the protected central beam. Though Test #1 showed a smaller maximum displacement than Test #3 due to the protected central beam, it failed to survive the 2-hour standard fire in both the simulation and the test due to the inadequate rebar area. Once the crack initiated, it propagated rapidly since the inadequate rebar cannot transfer the load across the cracks, and resulted in integrity failure and stopping of the test.

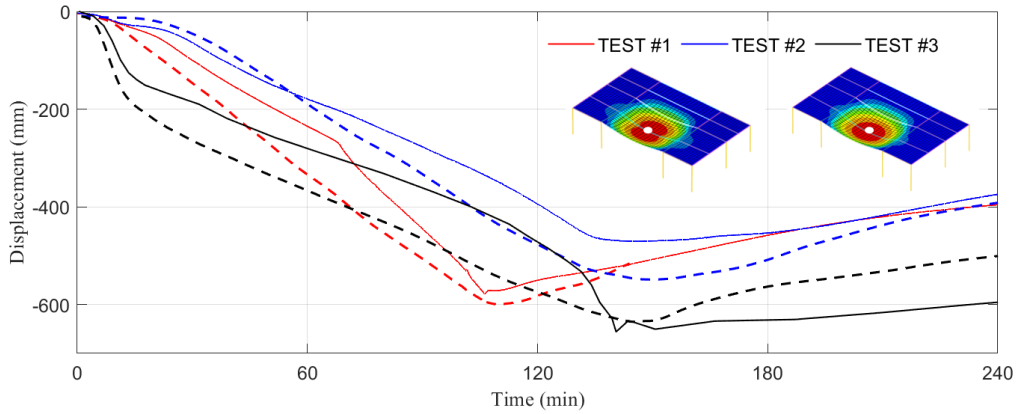

Figure 7. Comparison of vertical displacements at the center of the fire exposed composite floor for the three NIST experiments: measurements (solid lines) versus SAFIR model (dashed lines).

3.2.2 Damage distribution in concrete slab

The concrete shell model captures plasticity and damage. While it does not predict discrete crack openings, it computes a damage parameter in tension and compression at every point of integration in the shells. The damage parameter varies between zero and one, with one meaning that the material is fully damaged. In each shell element, there are 36 integration points (IP), distributed as four over the surface times nine across the thickness. Both the maximum value of the damage and the average over the 36 IP of the shell are plotted.

The distribution of damage within the concrete slab at 69 mins from the numerical models is plotted in Figure 8. The damage in the simulation of Test #1 predominantly concentrates above the central beam and around the slab edges. The max damage distribution pattern indicates that the damage is not effectively transferred to other parts of the slab, which contrasts with the damage distribution in Test #2. The increased rebar area in Test #2 not only reduces the peak damage values but also enhances the load transfer capabilities along the rebar, illustrating the effectiveness of increased rebar in mitigating concentrated damage. The comparison between the simulation of Test #2 and #3 reveals that the unprotected central beam contributes to a more evenly spread damage pattern across the slab. Besides, the maximum damage

value above the central beam is notably decreased compared to Test #2, indicating the critical role of central beam's fire protection on the concrete damage pattern.

In summary, the simulation of Test #1 exhibits a significant concentrated peak of damage near the central beam, aligning with the observed full-depth crack during the test. However, this is resolved by increasing the rebar area to spread the damage as evidenced by the simulated damage distribution of Tests #2 and #3.

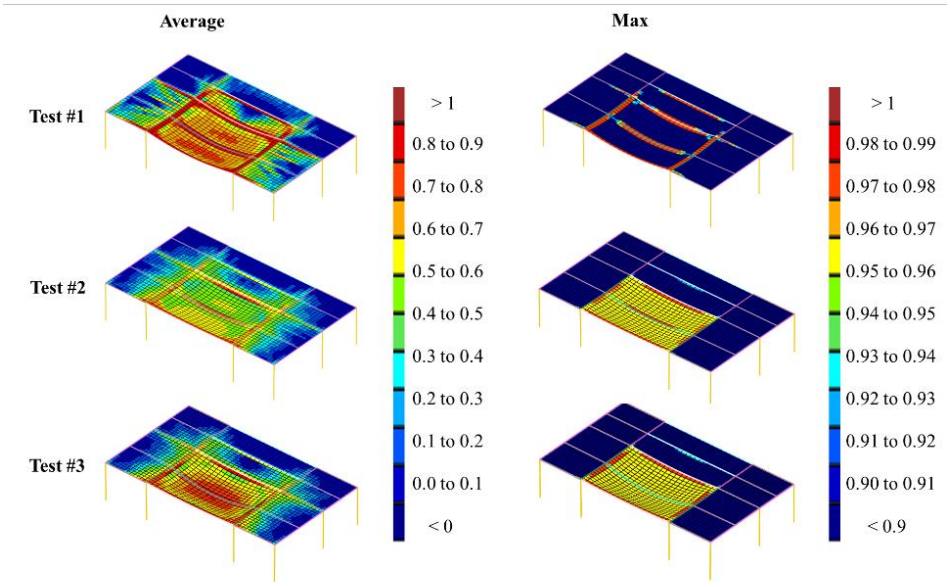

Figure 8. Computed distributions of damage (average and maximum values in each shell) in the concrete slab for the three tests at 69 mins. (Note: 69 min is the time of apparition of a large crack in Test #1).

3.2.3 Discussion on limit state

Figure 9 plots the computed concrete slab damage pattern at 2-hour and the post fire concrete crack patterns observed after the tests. The rebar failure pattern predicted by the simulation is also plotted. The simulation uses a stress-strain curve for the steel reinforcement that, after reaching the yield strength, plateaus up to a strain threshold of 0.05, beyond which the stress drops linearly to zero at 0.10 strain. Thus, failure of rebar is assumed once the strain in the rebars exceeds 0.05 (the steel is in the descending branch). For Test #1, the simulated concrete damage pattern aligns closely with the crack patterns observed in the test, and the simulation accurately predicts rebar failure locations above the central beam and at the north edge of the slab. For Test #2, a lot of small cracks (which closed upon cooling) were observed after the test but there was no rebar failure observed. Besides, more small cracks were observed at the south half of slab compared with the north half of the slab. This is also consistent with the observation in the numerical model. The simulation indicates a broader high damage zone (colored red) on the southern slab, with a maximum damage value significantly reduced from that of Test #1, suggesting effective load redistribution through the rebar network. For Test #3, the location of the observed concrete cracks correlates well with the high damage zone identified in the simulation. The consistency in the damage pattern between the test and simulation indicates that the numerical model can capture the concrete and rebar limit states of the tests.

Figure 10 plots the vertical displacement at slab center for the Test #1, with the black star marking the moment flame leakage was observed during the test, and a red star indicating the time of rebar failure in the simulation. It was noted during the test that the rupture of the steel rebar led to rapid expansion of the concrete crack, subsequently resulting in flame leakage. Therefore, rebar failure can serve as an indicator of potential flame leakage. The temporal alignment between the rebar failure and the onset of flame leakage underscores the effectiveness of the numerical model in accurately predicting the limit states, highlighting its potential as a predictive tool for assessing structural integrity under fire conditions.

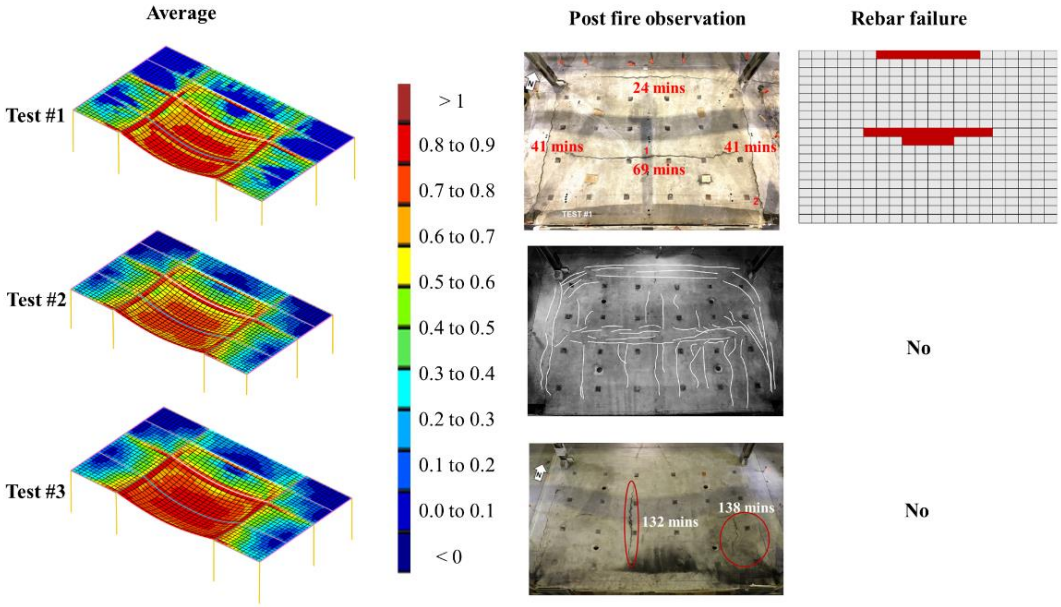

Figure 9. Comparison between observed cracks and computed distributions of damage (average and maximum values) in the concrete slab for the three tests at 2-hour. (Note: small cracks for test #2 are marked as white lines.)

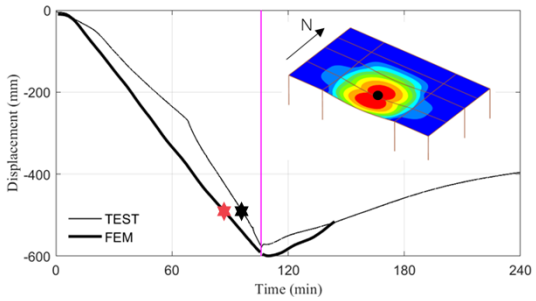

Figure 10. Vertical displacements at the center of the fire exposed composite floor for the Test #1. (Note: the pink line indicates the stop of the test.)

4 PARAMETRIC ANALYSIS

4.1 Minimum required slab rebar area

Both experimental and numerical findings highlight the critical role of slab rebar area in the fire response of the composite floor systems. A detailed analysis is performed to identify the minimum required rebar area for resisting 2-hour of standard ASTM E119 fire, focusing on avoiding reinforcement failure or simulation failures until the full cooling. Results are plotted in Figure 11. The analysis is conducted for the two different design approaches, namely the prescriptive (central beam protected, Test #1) and the performance-based design (central beam unprotected, Test #3). For Test #1, it is determined that increasing the rebar area from 60 mm^2/m to 100 mm^2/m allows the simulations to converge to the end without integrity failure. Although a rebar area of 80 mm^2/m allowed the simulation to converge until 180 mins, rebar failure is observed during the cooling phase. Therefore, a rebar area of 100 mm^2/m is identified as the minimum for the prescriptive design of this system (for the specific parameters considered here), which can distribute loads across cracks uniformly and avoid damage concentration at the existing cracks. It is important to note that the threshold of 100 mm^2/m is determined based on the same welded wire mesh used in the test, characterized by a yield stress of 755 MPa.

For the floors with unprotected central beam, the determined minimum rebar area is 170 mm^2/m to avoid integrity failure. Though the simulation with 150 mm^2/m of rebar area can run to the end, rupture of steel reinforcement is observed during cooling phase, indicating that this rebar level was insufficient for ensuring structural resilience throughout the entire test, including the cooling period. The steel grade used in Test #3 was S480. Therefore, the minimum amount of steel reinforcement for the floor with unprotected central beam is slightly higher (8% more when the S480 used in Test #3 is converted to S755 used in Test #1) than for floors with protected central beams. This suggests that removing fire protection from central beams, while still ensuring structural integrity for two hours, could offer cost and sustainability advantages. These conclusions pertain to the context of the NIST floor prototypes and 2-hour ASTM E119 fire, which are based on U.S. design practices.

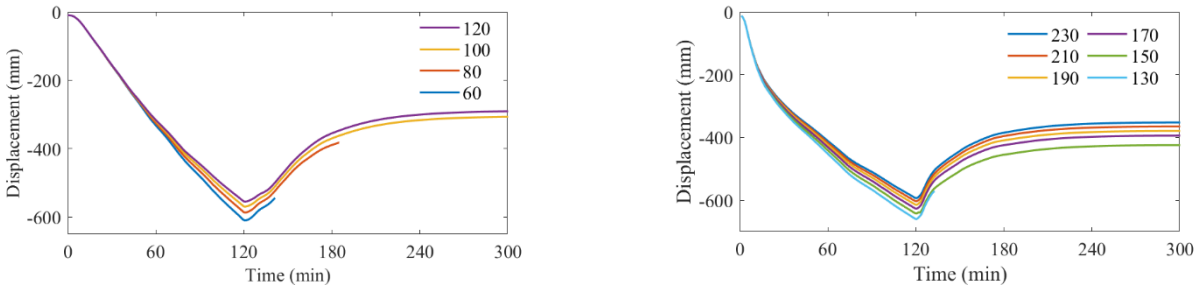

(a) NIST Test #1 (b) NIST Test #3

Figure 11. Central beam displacement as a function of the rebar areas (mm^2/m) in the slab, for the designs of (a) and (b).

4.2 Single slab model

The full building model in Section 3 accurately predicts the test observations but can be computationally expensive. This limits its application in probabilistic analyses, which requires running many simulations to account for variability and uncertainty in input parameters and conditions. For computational efficiency, an alternative model is developed, which excludes the surrounding slabs not exposed to the fire, as shown in Figure 12 (a). Translation in the x-direction is blocked to capture in a simplified manner the continuity of the concrete slab in that direction, which in the real structure restrains the thermal expansion.

The comparison of the vertical displacement between the single slab model and the test is shown in Figure 12 (b), indicating that the single slab model effectively captures the overall displacements. Unlike the full building model which shows an asymmetric response between the north and south beams due to surrounding bays, the single slab model shows a symmetrical displacement and damage pattern. Additionally, within the single slab model, the steel rebar and beams for Test #3 reach their limit strain, which is not observed in the full building model. This is expected to come from the beneficial effect of continuity at the boundaries in the full building model, known to improve the membrane action [14, 15].

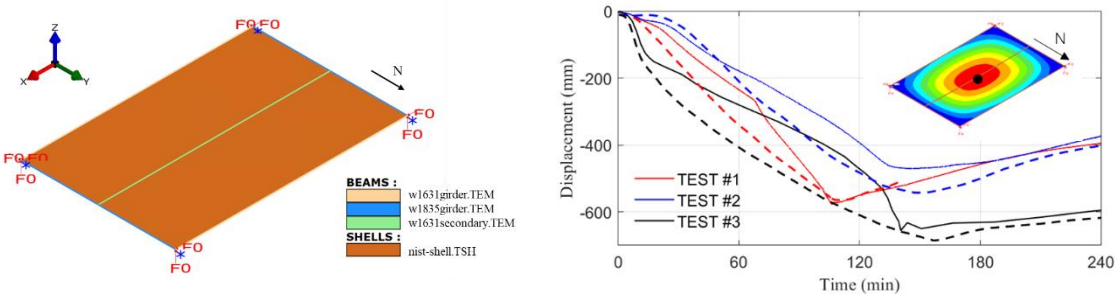

(a) Single slab model (b) Comparison of vertical displacement at slab center

Figure 12. Single slab model and correspond response.

While the single slab model may not achieve the same level of precision as the full building model in predicting the damage pattern, it provides a satisfactory prediction on the overall displacement response of the floor system. Crucially, the single slab model can reduce the computational cost significantly (for Test #1, the computation time of single slab model is 22% of the full building model), which is particularly advantageous for conducting probabilistic analyses.

5 PRELIMINARY STUDY ON THE FRAGIILITY CURVES

5.1 Selection of Probabilistic Parameters

Probabilistic structural fire analyses are conducted under natural fires. Uncertainties in five parameters are considered. The opening factor is taken as a random variable. Uncertainties in temperature-dependent thermal properties (thermal conductivity, specific heat, density) of the sprayed fire resistive material (SFRM) and the mechanical properties of the steel for the beams are also considered based on the equations proposed in [7]. In addition, the fire load is varied in the range 100-2100 MJ/m^2, as the intensity measure.

5.2 Definition of Damage States

Five damage states are defined. The criteria for defining damage states zero to three are based on the residual vertical deflection Δ_s after the end of the fire [16], see Table 1. Damage state four is taken as the integrity failure of the floor. This is defined in the numerical model as lack of convergence due to either failure of the steel reinforcement or runaway vertical deflections.

Table 1 Definition of damage states for the composite floor system.

Damage state	0	1	2	3	4
Criterion	$\Delta_s/l \leq 1/240$	$1/240 \leq \Delta_s/l < 1/120$	$1/120 \leq \Delta_s/l < 1/60$	$1/60 \leq \Delta_s/l$	$1/60 \leq \Delta_s/l$ and (non-convergence or steel failure)

Remark: Δ_s is the residual vertical deflection at the center of the lab. $l = \sqrt{l_1 l_2}$ where l_1 and l_2 are the spans of slab.

5.3 Development of Fragility Curves

The fragility curves are developed to depict the exceedance probability of the damage states and are conditional to the fire load. To generate the fragility points $P(DS = DS_i|q_m)$ for DS_i under a given fire load q_m, fire-thermo-mechanical analyses are conducted with the non-linear FE model. Between 10 to 30 simulations are run at each fire load level taken between 100 MJ/m^2 to 2100 MJ/m^2 with a step ranging from 50 MJ/m^2 to 200 MJ/m^2. Once the fragility points at different fire loads are generated, the fragility curves are fitted using a two-parameter lognormal distribution function, as given in Eq. (1).

$$\mathrm{FFs}(DS_i|\mathrm{q}) = P(DS \geq DS_i|q) = \Phi\left[\frac{\ln(\mathrm{MinMaxScaler}(q)) - \mu}{\sigma}\right] = \frac{1}{2}\left[1 + \mathrm{erf}\left(\frac{\ln\left(\frac{q-q_{min}}{q_{\max}-q_{min}}\right)-\mu}{\sigma\sqrt{2}}\right)\right] \quad (1)$$

where Φ is the standardized cumulative normal distribution function, $\mathrm{MinMaxScaler}(q)$ normalizes the fire load to range [0, 1], with $q_{min} = 100\ \mathrm{MJ}/m^2$ and q_{max}=2100 MJ/m^2, erf is the Gauss error function, μ and σ are two parameters characterizing the fragility functions and are determined by maximizing the best fit with the data from the analysis.

5.4 Results

Fire fragility curves are established for the three NIST prototypes based on the single slab model introduced in Section 4.2. The curves are shown in Figure 13.

The comparison between the Test #3 and Test #1 indicates that the Test #3 (PBD) has a higher probability of reaching mild and moderate damage than the Test #1 (prescriptive) when the fire load ranges from 100

to 1000 MJ/m^2, but a much lower probability of reaching DS4 (integrity failure) when the fire load lies between 700 to 2100 MJ/m^2. This is because the development of TMA in Test #3 relies on large deflections, resulting in a higher likelihood of damage states 1-3 compared with the prescriptive design. Yet the development of TMA at large deflection successfully prevents excessive localized damage and wire rupture on the slab center, preventing the early development of full-depth cracks as observed in the NIST experiment, and therefore reducing the probability of integrity failure. The design based on TMA is thus more robust under natural fires than the current prescriptive design.

The comparison of the DS4 fragility curve for Test #2 and #3 reveals that, for the same rebar area, a composite floor with unprotected central beams is more likely to experience integrity failure than a floor with protected central beams once the fire load becomes higher than 1100 MJ/m^2.

It is important to note that the above conclusions pertain to the context of the NIST floor prototypes, which are based on U.S. design practice.

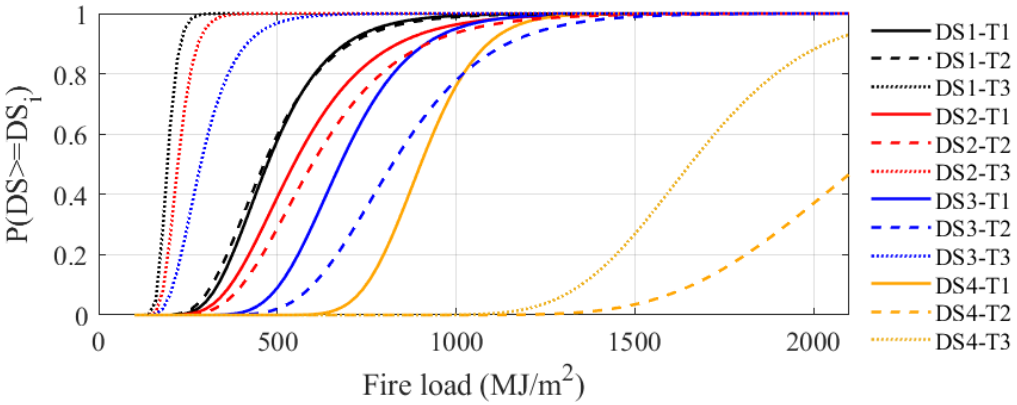

Figure 13: Fragility curves for the three prototypes of composite floors tested by the NIST.

6 CONCLUSION

This study conducted a finite element (FE) analysis of steel-concrete composite floors, leveraging data from three full-scale fire tests at NIST to evaluate the U.S. prescriptive design and performance-based design methods. The three experiments included a prescriptive fire design (#1), a design with enhanced steel reinforcement in the slab (#2), and a design with enhanced reinforcement but without fire protection on the central steel beam (#3). The main conclusions are summarized below.

The study reveals that the minimum permitted rebar area of 60 mm^2/m in current U.S. prescriptive design codes may not be sufficient for two-hour fire resistance of the system, as evidenced by the observed integrity failure in both the experiment and the FE model. For designs with enhanced reinforcement (#2) and unprotected central beam (#3), both the experiment and FE model show the survival of the composite floor system until the end of the test. The FE models successfully predict the limit states and capture the beneficial effects of tensile membrane action and the importance of adequate steel reinforcement in composite floor systems.

The numerical study determined the minimum reinforcement necessary to avoid integrity failure until the full cooling. For the prescriptive design, an increase from 60 mm^2/m to 100 mm^2/m of the S755 mesh is required to survive the 2-hr ASTM E119 fire. For the performance-based design, the minimum amount of S480 rebars is 170 mm^2/m to develop tensile membrane action with unprotected central beam and survive the fire exposure. Using a consistent steel grade for comparison, the minimum amount for the performance-based design would be 108 mm²/m of S755 mesh, thus only a limited increase from the prescriptive design to offset the removal of insulation on the central beam.

Additionally, a single slab FE model is established and shown to be a good trade-off between accuracy and computational efficiency for use in probabilistic studies. This single slab model is used for constructing fragility curves for the three NIST prototypes under physically based (i.e., natural) fires. The results indicate that Test #3 (PBD) with unprotected central beam has a higher likelihood of experiencing mild and

moderate damage than Test #1 (prescriptive) but a lower probability of experiencing failure. This is because the development of tensile membrane action relies on large deflections, but on the other hand offers a robust load path. The developed fragility curves will be used in future studies on lifetime cost analysis.

ACKNOWLEDGMENTS

This work was performed under the following financial assistance award 60NANB22D110 from U.S. Department of Commerce, National Institute of Standards and Technology. This support is gratefully acknowledged. The statements, findings, conclusions, and recommendations are those of the authors and do not necessarily reflect the views of the NIST or the U.S. Department of Commerce.

REFERENCES

[1] C.G. Bailey, Membrane action of slab/beam composite floor systems in fire, Engineering Structures 26(12) (2004) 1691-1703.
[2] T. Gernay, Performance-based design for structures in fire: Advances, challenges, and perspectives, Fire Safety Journal 142 (2024) 104036.
[3] L. Choe, S. Ramesh, X. Dai, M. Hoehler, M. Bundy, R. Bryant, B. Story, A. Chakalis, A. Chernovsky, Fire resilience of a steel-concrete composite floor system: full-scale experimental evaluation for US Prescriptive approach with a 2-hour fire-resistance rating (test# 1), Technical Note (NIST TN), National Institute of Standards and Technology, Gaithersburg, MD, 2021.
[4] L. Choe, M. Hoehler, M. Bundy, R. Bryant, B. Story, A. Chakalis, A. Chernovsky, S. Ramesh, X. Dai, Fire resilience of a steel-concrete composite floor system: full-scale experimental evaluation for influence of slab reinforcement (test# 2), Technical Note (NIST TN), National Institute of Standards and Technology, Gaithersburg, MD, 2022.
[5] S. Ramesh, L. Choe, M. Hoehler, M. Bundy, R. Bryant, G.D.C. Torres, B. Story, A.R. Chakalis, A.A. Chernovsky, P. Deardorff, Fire Resilience of a Steel-Concrete Composite Floor System: Full Scale Experimental Evaluation for Influence of Slab Reinforcement and Unprotected Secondary Beam (Test# 3), Technical Note (NIST TN), National Institute of Standards and Technology, Gaithersburg, MD, 2023.
[6] J.-M. Franssen, T. Gernay, Modeling structures in fire with SAFIR®: Theoretical background and capabilities, Journal of Structural Fire Engineering 8(3) (2017) 300-323.
[7] N. Elhami Khorasani, P. Gardoni, M. Garlock, Probabilistic fire analysis: material models and evaluation of steel structural members, Journal of Structural Engineering 141(12) (2015) 04015050.
[8] C. Ma, T. Gernay, Numerical analysis of full-scale structural fire tests on composite floor systems (Under review), Fire safety journal (2024).
[9] EN1994-1-2, Eurocode 4: Design of composite steel and concrete strucutres - Part 1-2: General rules-Structural fire design, 2005.
[10] J. Jiang, J.A. Main, J.M. Weigand, F. Sadek, Reduced-order modeling of composite floor slabs in fire. I: Heat-transfer analysis, Journal of Structural Engineering 146(6) (2020) 04020080.
[11] EN1992-1-2, Eurocode 2: Design of Concrete Structures - Part 1-2: General rules - Structural fire design, 2004.
[12] T. Gernay, A. Millard, J.-M. Franssen, A multiaxial constitutive model for concrete in the fire situation: Theoretical formulation, International Journal of Solids and Structures 50(22-23) (2013) 3659-3673.
[13] S. Ni, T. Gernay, Considerations on computational modeling of concrete structures in fire, Fire Safety Journal 120 (2021) 103065.
[14] T. Gernay, N.E. Khorasani, Recommendations for performance-based fire design of composite steel buildings using computational analysis, Journal of Constructional Steel Research 166 (2020) 105906.
[15] J. Jiang, H. Qi, Y. Lu, G.-Q. Li, W. Chen, J. Ye, A state-of-the-art review on tensile membrane action in reinforced concrete floors exposed to fire, Journal of Building Engineering 45 (2022) 103502.
[16] S. Ni, T. Gernay, A framework for probabilistic fire loss estimation in concrete building structures, Structural Safety 88 (2021) 102029.